# *Coherent Multilateral Radar Processing for Precise Target Geolocation*

# Coherent Multilateral Radar Processing for Precise Target Geolocation[1]

Jen King Jao
MIT Lincoln Laboratory, 244 Wood St, Lexington, MA 02420-9108, E-mail: Jao@ll.mit.edu

*Abstract*—**This paper analyzes the target geolocation performance of coherent processing of target signals observed by several radar receivers in a multilateral configuration. Each radar sensor is designed with a sufficient bandwidth to support good target range resolution but without the benefit of a narrow radar antenna beam for useful cross range measurement of the target position. The analysis results demonstrate the ability of coherent multilateral radar signal processing to achieve accurate target geolocation via triangulation and to eliminate target ghosts in a dense, multiple target environment.**

**Index Term–multilateral MIMO radar, multiple target tracking, target geolocation, target ghost mitigation**

## I. INTRODUCTION

The rapid evolution of UAV technology has stimulated strong interest in the development of airborne radar surveillance systems based on small, low-cost platforms. Despite many potential utilities in persistent intelligence, surveillance, and reconnaissance of ground moving targets, the capability of a small GMTI radar platform is often constrained in design by its physical size. A small platform typically offers very limited space that prohibits the installation of a large radar antenna. Thus, the resultant antenna beam, with its beamwidth inversely proportional to the antenna aperture in units of the radar wavelength, will illuminate a large far-field angular footprint on the ground. One undesirable consequence of a large antenna beamwidth is its inability to support accurate measurement of the target cross range position. For example, the combination of an operational X-band radar wavelength of 0.03 m at 10 GHz and an antenna aperture size of 0.3 m results in a radar beamwidth of 5.7 deg. Given this beamwidth and a beam splitting ratio of 10 at a relatively high target signal-to-noise ratio of 20 dB, the target cross range measurement uncertainly will be on the order of 400 m at the range of 40 km and worse at a longer range. The large target position estimation error will probably fail to produce a clear situational picture that displays accurate target locations in the surveillance space.

One potential remedy to overcome the above shortcoming is to deploy multiple radar sensor platforms where each sensor is operated with a sufficient bandwidth to provide good target range information. The idea is that, via triangulation, target range measurements from multiple sensors will determine the target location under suitable geometry. Indeed, accurate range measurements from at least two radar sensors, whose line-of-sight vectors intercept the target at a large bistatic angle, can be triangulated to uniquely locate the spatial location of a single isolated target without the benefit of cross-range measurement [1]. Unfortunately, when multiple targets are present, it is no longer plausible that all the target positions can be unambiguously derived from the target-to-sensor range measurements. This point is illustrated by Fig. 1. This figure depicts the situation of three targets observed by two radars that provide good measurements only in range but not cross range under the assumption of large antenna beamwidths for both radars. In the figure, it is clear that a total of nine potential locations may be assigned to the three targets via triangulation; three are true target locations whereas the other six are erroneous ghosts. Thus, in a dense target environment, geometric triangulation may erroneously assign many targets to their ghost locations [2]. The potential ghost sites can be large and, in the large-number limit, increase almost as fast as the square of the number of targets. If the target ghosts are not eliminated, it will be difficult to discern the actual number of real targets and to unambiguously determinate their locations.

Fortunately, unambiguous resolution of actual target detections and their position measurements can be achieved by coherent multilateral radar signal processing. Qualitatively, the error of position estimation will be on the order of one radar range resolution length in both range and cross range. In this paper, coherent multilateral radar signal processing will be analyzed to demonstrate its application to precision target geolocation. The organization of this paper is as follows. In Section 2, a multilateral radar signal data model will be defined. Then, in Section 3, the outputs of three signal processing schemes are derived. Based on these models,

[1] This work was sponsored by the Defense Advanced Research Project Agency, Information Exploitation Office under US Air Force Contract FA8721-05-C-0002. Opinions, interpretations, conclusions, and recommendations are those of the author and are not necessarily endorsed by the United States Government.

0-7803-9497-6/06/$20.00 © 2006 IEEE.

Section 4 presents numerical results of several simulation examples. Section 5 and 6 present general discussions and conclusion of these results.

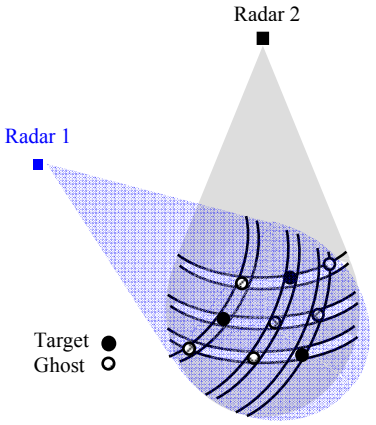


Fig. 1 Observation of multiple targets and ghosts.

## II. RADAR SIGNAL AND DATA MODEL

Generally, the multilateral radar signal properties vary with the radar-target geometry and the target scattering and signal propagation environment. Due to the complexity of the radar phenomenology involved, it is not possible to investigate the details of all possibilities. In this paper, certain simplifying assumptions are made to highlight only the pertinent features related to the subject at hand. For the present purpose, we assume a system of $M$ radars, reminiscent to the configuration in Fig. 1, that interrogate $N$ stationary targets in free space. Each radar utilizes the same waveform of sufficient bandwidth such that its receiver IF output is characterized by a single range compression filter response $\phi$. However, each radar waveform is assumed to be operated in a disjoint band. For example, the *mth* radar band may be centered at a different but adjacent frequency $f_m$, $m = 1, 2, \ldots M$. This assumption is not a requirement but conveniently adopted as an example to ensure proper operation of the whole radar system. The radar system response at the position $\boldsymbol{r}$ after a single coherent processing interval is represented by the $M$-dimensional data vector $\boldsymbol{z}(\boldsymbol{r}) = [z_1, \ldots z_m, \ldots z_M]^T$ and each element $z_m(\boldsymbol{r})$ is the resultant sum over $N$ targets, located at $\boldsymbol{r}_n$, $n = 1, 2, \ldots N$, such that

$$
\begin{aligned}
& z_m(\boldsymbol{r}) = \sum_{n=1}^{N} b_n \, \phi_{mn}(\boldsymbol{r}) v_m(\boldsymbol{r}) + w_m \quad ; \\
& \phi_{mn}(\boldsymbol{r}) = \rho_{mn} \sqrt{(SNR)_{mn}} \, \phi\big(R_m(\boldsymbol{r}) - R_m(\boldsymbol{r}_n)\big) \\
& R_m(\boldsymbol{r}) = \left|\boldsymbol{r} - \boldsymbol{q}_m\right| \quad ; \quad v_m(\boldsymbol{r}) = \exp\big(i 2 k_m R_m(\boldsymbol{r})\big).
\end{aligned}
\tag{1}
$$

Here, the variable $R_m(\boldsymbol{r})$ measures the slant range between a vector position $\boldsymbol{r}$ and the *mth* radar position $\boldsymbol{q}_m$. The signal phase due to free-space propagation from $\boldsymbol{r}$ to $\boldsymbol{q}_m$ is sampled by $v_m(\boldsymbol{r}) = \exp(i 2 k_m R_m(\boldsymbol{r}))$, $k_m = 2\pi/\lambda_m$. The variable $\phi_{mn}(\boldsymbol{r})$, that represents the *nth* target backscatter signal impinging on the *mth* radar receiver, is given by the product of a complex coefficient $\rho_{mn}$ of unity magnitude, the signal amplitude, scaled by the square root of the target signal-to-noise ratio $(SNR)_{mn}$, and the range compression filter response $\phi(R_m(\boldsymbol{r}) - R_m(\boldsymbol{r}_n))$. The coefficient $\rho_{mn}$, that represents the signal phase of the *nth* target backscatter as observed by the *mth* radar, has absorbed the propagation phase factor $\exp(-i 2 k_m R_m(\boldsymbol{r}_n))$. The amplitude fluctuation of the *nth* target backscatter is denoted by $b_n$. The correlation between a target pairs is given by the element $b_{mn} = E(b_m b_n^*)$ with $E(|b_n|^2) = 1$ of the matrix $\boldsymbol{B} = E(\boldsymbol{b}\boldsymbol{b}^H)$, $\boldsymbol{b} = [b_1, b_2, \ldots b_N]^T$. In vector notation, (1) becomes

$$
\begin{aligned}
& \boldsymbol{z}(\boldsymbol{r}) = \boldsymbol{A}\,\boldsymbol{b} + \boldsymbol{w} \quad ; \\
& \boldsymbol{A} = \left[\boldsymbol{v}(\boldsymbol{r}) \cdot \boldsymbol{\varphi}_1(\boldsymbol{r}) \ldots \boldsymbol{v}(\boldsymbol{r}) \cdot \boldsymbol{\varphi}_n(\boldsymbol{r}) \ldots \boldsymbol{v}(\boldsymbol{r}) \cdot \boldsymbol{\varphi}_N(\boldsymbol{r})\right] \\
& \boldsymbol{v}(\boldsymbol{r}) = \left[v_1(\boldsymbol{r}) \ldots v_m(\boldsymbol{r}) \ldots v_M(\boldsymbol{r})\right]^T \\
& \boldsymbol{\varphi}_n(\boldsymbol{r}) = \left[\phi_{1n}(\boldsymbol{r}) \ldots \phi_{mn}(\boldsymbol{r}) \ldots \phi_{Mn}(\boldsymbol{r})\right]^T \\
& \boldsymbol{b} = \left[b_1 \ldots b_n \ldots b_N\right]^T \quad .
\end{aligned}
\tag{2}
$$

In (2), the matrix $\boldsymbol{A}$ consists of $N$ $M$-dimensional vectors $\boldsymbol{v}(\boldsymbol{r}) \cdot \boldsymbol{\varphi}_n(\boldsymbol{r})$, $n = 1, 2, \ldots N$, that in term of element-wise multiplication is the Hadamard product of two vectors, $\boldsymbol{v}(\boldsymbol{r})$ and $\boldsymbol{\varphi}_n(\boldsymbol{r}) = [\phi_{1n}\ \phi_{2n} \ldots \phi_{Mn}]^T$. The data vector $\boldsymbol{z}$ is normalized such that the $M$ white noise components $w_m$ of $\boldsymbol{w} = [w_1, w_2 \ldots w_M]^T$ are regarded as independent, identical, and complex Gaussian with an identity covariance matrix $E(\boldsymbol{w}\boldsymbol{w}^H) = \boldsymbol{I}_M$. Thus, the covariance matrix $\boldsymbol{R}_z$ of $\boldsymbol{z}$ and its inverse $\boldsymbol{R}_z^{-1}$ can be shown from (2) to be

$$
\begin{aligned}
& \boldsymbol{R}_z = \mathrm{E}\left(\boldsymbol{z}(\boldsymbol{r})\boldsymbol{z}^H(\boldsymbol{r})\right) = \boldsymbol{A}\boldsymbol{B}\boldsymbol{A}^H + \boldsymbol{I}_M \quad ; \\
& \boldsymbol{R}_z^{-1} = \boldsymbol{I}_M + \boldsymbol{A}\left(\boldsymbol{B}^{-1} + \boldsymbol{A}^H\boldsymbol{A}\right)^{-1}\boldsymbol{A}^H \quad .
\end{aligned}
\tag{3}
$$

## III. SIGNAL PROCESSING APPROACHES

Three processing schemes are analyzed here. The first approach is the noncoherent averaging of multiple radar signals that generalizes the concept of multilateral range triangulation. The output of this process is

$$
\begin{aligned}
\frac{1}{M} E\left(\left|\boldsymbol{z}(\boldsymbol{r})\right|^2\right) &= 1 + \frac{1}{M} tr\left(\boldsymbol{A}\boldsymbol{B}\boldsymbol{A}^H\right) = 1 + \frac{1}{M} tr\left(\boldsymbol{\Phi}\boldsymbol{B}\boldsymbol{\Phi}^H\right) \\
&= 1 + \frac{1}{M} \sum_{i=1}^{N} \sum_{j=1}^{N} b_{ij} \boldsymbol{\varphi}_j^H(\boldsymbol{r}) \boldsymbol{\varphi}_i(\boldsymbol{r}) \\
\boldsymbol{\Phi}(\boldsymbol{r}) &= \left[\boldsymbol{\varphi}_1(\boldsymbol{r}) \ldots \boldsymbol{\varphi}_n(\boldsymbol{r}) \ldots \boldsymbol{\varphi}_N(\boldsymbol{r})\right] \quad .
\end{aligned}
\tag{4}
$$

The second approach is essentially backprojection that coherently integrates all the multilateral radar signals by averaging over multiple coherent processing intervals the squared inner product $\boldsymbol{v}^H(\boldsymbol{r})\boldsymbol{z}(\boldsymbol{r})$ of the data vector $\boldsymbol{z}$ and a

"steering vector" $\boldsymbol{v}$. The steering vector $\boldsymbol{v}$ compensates the hypothetical target signal phase propagating along the slant range vector from $\boldsymbol{r}$ to $\boldsymbol{q}_m$. In term of the covariance $\boldsymbol{R}_z$, the integrated output is

$$\begin{aligned}
&\frac{1}{M}E\left(\left|\boldsymbol{v}^H(\boldsymbol{r})z(\boldsymbol{r})\right|^2\right)=\frac{1}{M}\boldsymbol{v}^H(\boldsymbol{r})\,\boldsymbol{R}_z\,\boldsymbol{v}(\boldsymbol{r})\\
&=1+\frac{1}{M}\boldsymbol{e}^H\left(\boldsymbol{\Phi}\boldsymbol{B}\boldsymbol{\Phi}^H\right)\boldsymbol{e}\\
&=1+\frac{1}{M}\sum_{i=1}^{N}\sum_{j=1}^{N}b_{ij}\left(\boldsymbol{e}^H\boldsymbol{\varphi}_i(\boldsymbol{r})\right)\left(\boldsymbol{\varphi}_j^H(\boldsymbol{r})\boldsymbol{e}\right)\\
&\boldsymbol{e}=\left[1\ 1\ \ldots\ 1\right]^T\ ;\ M\text{ x }1\text{ vector}.
\end{aligned}\tag{5}$$

The expression on the left hand side of the first line in (5) defines the coherent receiver signal processing operation. Other coherent processing techniques also can be useful such as the Minimum Variance Distortionless Response (MVDR) beamformer output given by

$$\text{MVDR}=\frac{M}{\boldsymbol{v}^H(\boldsymbol{r})\,\boldsymbol{R}_z^{-1}\,\boldsymbol{v}(\boldsymbol{r})}\tag{6}$$

The MVDR process can enhance the target response provided the signal processing chains in all radar receivers are properly calibrated and equalized. Although the backscatters from a target pair are generally correlated and the off-diagonal matrix elements $b_{ij} = E(b_i b_j^*)$ of $\boldsymbol{B}$ do not always vanish, independent targets will be assumed in the following exercises such that $b_{ij} = \delta_{ij}$ unless stated otherwise. Under this assumption, (4) and (5) are simplified to be

$$\begin{aligned}
&\text{Noncoherent output}=1+\frac{1}{M}\sum_{n=1}^{N}\left|\boldsymbol{\varphi}_n(\boldsymbol{r})\right|^2\ ;\\
&\text{Coherent output}=1+\frac{1}{M}\sum_{n=1}^{N}\left|\boldsymbol{e}^H\boldsymbol{\varphi}_n(\boldsymbol{r})\right|^2\ .
\end{aligned}\tag{7}$$

## IV. SIMULATION RESULTS

Simulation results according to the above signal models are presented in Figs. 2 through 8. Figure 2 plots the results for the case of two independent targets resolved by two stand-off radar receivers at far range. One is located toward the west while the other is directed in the northeast direction. The range compression filter response $\phi$ is computed as the Fourier transform of the frequency passband shaped by the Hamming window. In this figure, the spatial scale is normalized in the unit of one range resolution length equal to half of the product of the light speed and the inverse bandwidth. The *SNR* of each individual target signal component seen by both radars is taken to be 20 dB. Note that the output of the noncoherent processor, displayed in Fig. 2(a), indicates identical *SNR* peaks of 20 dB at four locations. Two peaks coincide with the true target locations marked with black crosses while the other two of equal intensity are spurious target ghosts. The target ghosts may be suppressed by coherent processing. The coherent backprojection and MVDR outputs in Fig. 2(b) and 2(c) both yield the *SNR* of 23 dB at the true target locations. In contrast, the *SNR* of two target ghosts are 20 dB. The MVDR output, shown in Fig. 2(c), further suppresses the spurious sidelobes in the target neighborhood. Figure 3 reinforces the simulation results for ten independent targets under radar illumination from the same directions as assumed in Fig. 2. Figure 3(a) reveals many target ghosts in the noncoherent processor output. In contrast, Figs. 3(b) and 3(c) highlight again the advantage of coherent processing to increase the target SNR relative to that of the ghosts. The benefit of coherent gain in the target *SNR* is very apparent. By coherently combining $M$ radar receiver outputs, the net *SNR* gain will be $M$ due to the total signal gain of $M^2$ at the expense of increasing the noise power by a factor of $M$. Note that given a dense ensemble of $N$ targets, the number of false targets on the order $N^2$-$N$ could potentially present a very confusing and erroneous picture of the target situation display.

The above simulations have assumed $\boldsymbol{B} = \boldsymbol{I}_M$ and also a unity phase coefficient $\rho_{mn}=1$ for all combination of $n$ and $m$. These simplified assumptions can not be universally valid in a realistic radar operational environment. In fact, multilateral coherent processing outputs will be affected by the cross correlation of different target backscatters and the signal phase statistics of $\rho_{mn}$ that are functions of such variables as the target type, scattering aspect angle, radar frequency, propagation medium, and geometry. As an example, the special case of two completely correlated targets with $b_{12} = b_{21} = 1$ is illustrated by Fig. 4(a). These targets and their associated ghosts can not be distinguished as now two targets behave essentially as one. Figure 4(b) illustrates the opposite case of two targets of negative unity correlation $b_{12} = b_{21} = -1$ that completely eliminates the ghost response. Figure 5 illustrates the effects of the target signal phase as observed by different radars. In this example, $\rho_{11} = \rho_{12}$ are fixed at unity but $\rho_{21}$ and $\rho_{22}$ are varied by tuning the phase angle of the target signals observed by the second radar relative to that of the first. Three cases of (a) in-phase, (b) partially in-phase, and (c) out-of-phase radar signals are simulated by setting $\rho_{21} = \rho_{22}$ to be respectively $\exp(i\pi/4)$, $\exp(i\pi/2)$, and $\exp(i\pi)$. Note that the result in Fig. 5(a) is very similar to Fig. 2(b) except for a slight drop of the target SNR. However, as the differential phase of different radar signals increases, the coherent processor may not be able to distinguish the real targets from their ghosts to the extent that the latter may actually be enhanced. These cases are illustrated by Fig. 5(b) and 5(c).

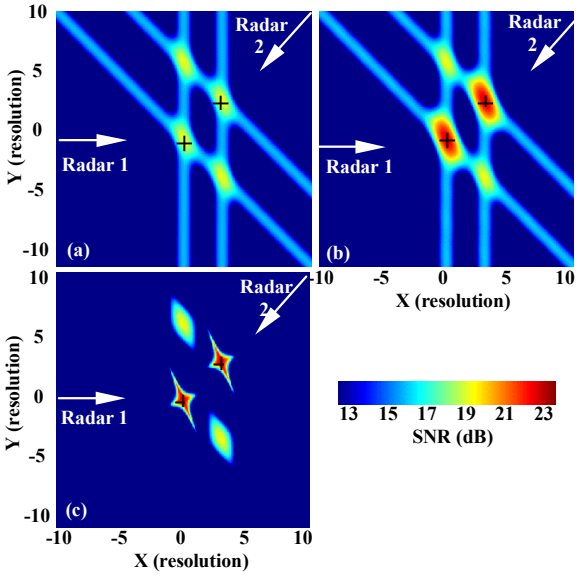


Fig. 2 Outputs of (a) noncoherent, (b) coherent, and (c) MVDR processing for the case of two targets and two radars.

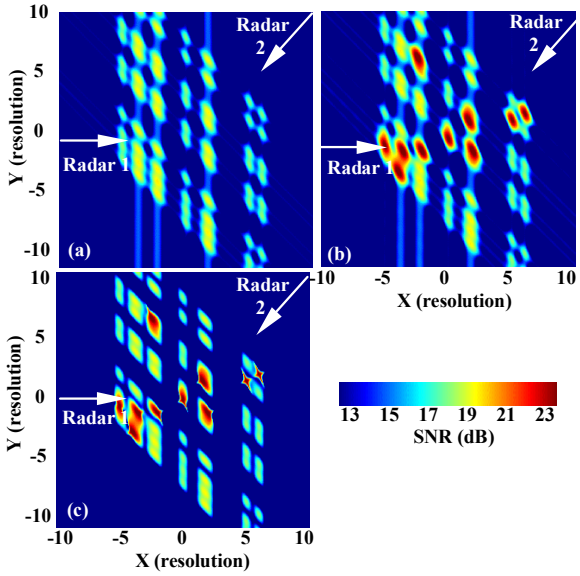


Fig. 3 Outputs of (a) noncoherent, (b) coherent, and (c) MVDR processing for the case of ten targets and two radars.

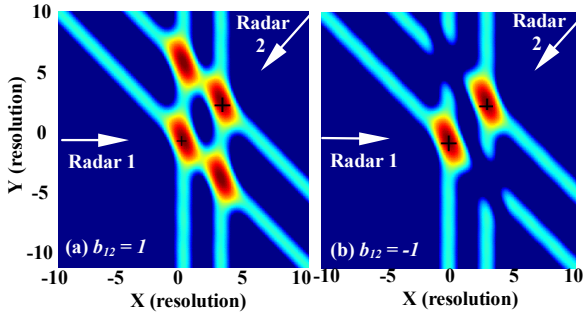


Fig. 4 Coherent processing outputs for two targets with (a) positive ($b_{12} = 1$) and (b) negative ($b_{12} = -1$) correlation.

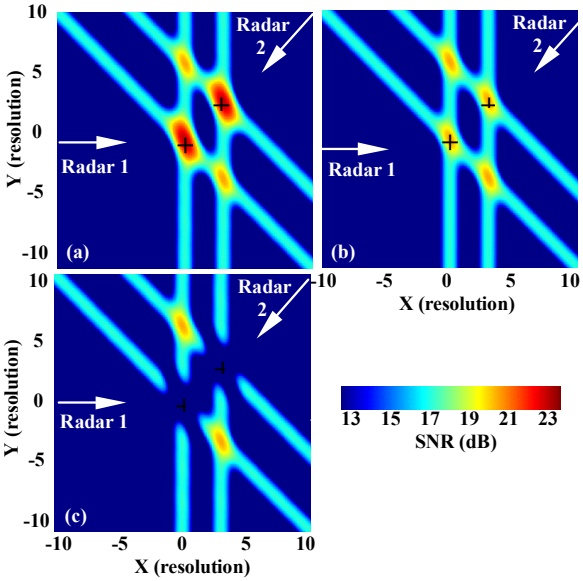


Fig. 5 Coherent processing outputs for (a) in-phase (b) patially in-phase, and (c) out-of-phase radar target signals.

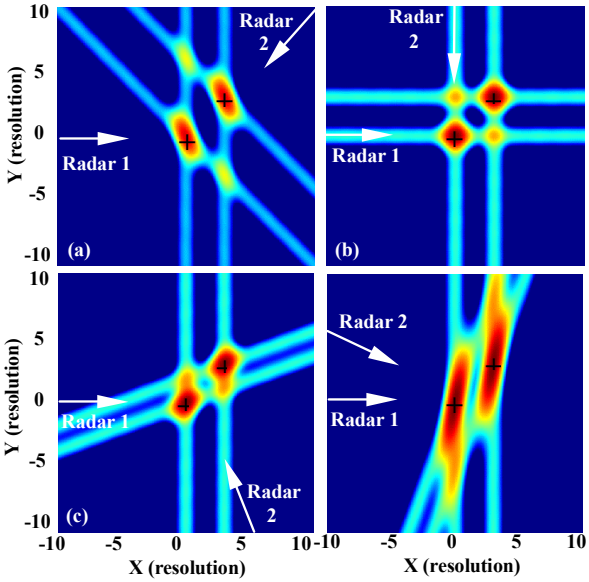


Fig. 6 Coherent processing outputs for different angular position of the second radar at (a) 45, (b) 90, (c) 160, and (d) 290 degrees from the target scene center.

Figures 6 through 8 simulate the impact of radar configuration. Again, independent targets and in-phase radar signals such that $b_{12} = b_{21} = 0$ and $\rho_{mn} = 1$ are hypothesized.In Fig. 6, the coherent backprojection outputs are displayed for four different radar arrangements. The first stand-off radar is toward the west whereas the second radar is placed (a) 45, (b) 90, (c) 160, and (d) 290 degree away from the target scene. In the latter two cases, the target and the ghosts start to merge with each other such that the cross range resolution of the targets' positions will be degraded. Figure 7 illustrates the

configuration of three stand-off radars by adding one southward from the target field. In this configuration, even noncoherent averaging may marginally distinguish the targets from their ghosts as shown in Fig. 7(a). Here, the average radar target SNR of 20 dB is slightly above the ghost SNR of 18.2 dB. The latter number is the result of adding two radar signal powers at the expense of tripling the noise power. However, in Fig. 7(b) or 7(c), higher target SNR of 24.7 dB is attained via either coherent backprojection or MVDR processing due to the integration gain of 3 or 4.77 dB. Thus the targets's level are 6.25 dB stronger than the ghosts' level. The number of target ghosts is given by $N(N-1)M(M-1)/2$ by counting combinatorial pairs of radar line-of-sight interceptions. The last example in Fig. 8 illustrates the case of ten independent targets observed by the same system of three radars. The results for (a) noncoherent average, (b) coherent, and (c) MVDR processing again demonstrate the superior capability of coherent processing for precise target geolocation and ghost mitigation.

## V. DISCUSSION

The above results have illustrated the potential benefits of coherent multilateral processing in resolving the real targets from their ghosts and in deriving accurate cross-range positions from targets' range measurements. However, the simulation exercises have adopted a number of simplified assumptions such as independent targets and well behaved target signal phases as modeled by the correlation matrix $\boldsymbol{B}$ and $MN$ coefficients $\rho_{mn}$. Presumably, these statistical variables are complex functions of target type, scattering angle, radar configuration and frequency, the propagation medium, and geometry. The need to better understand the physical phenomena related to multilateral signal processing is clear. Unfortunately, the knowledge of the multilateral radar target and propagation phenomenology and their measurement data base are at the present time immature. Thus, the task of accurate modeling of the target and propagation statistics are best relegated to the future when more data becomes available. The targets in the above analysis have been treated as stationary in free space. This practice allows this paper to focus on the essential issues of multilateral radar target geolocation without digression into the discussions of multilateral radar detection. However, in certain radar applications, target detection should not be taken for granted and it may not be always appropriate to regard target position estimation as a separate follow-on process. One such application could be the GMTI detection and geolocation of slowly moving targets. This is one area of multilateral radar research that will require further investigation.

In addition, the above formulation has conveniently assumed a system of multiple monostatic radar configurations.

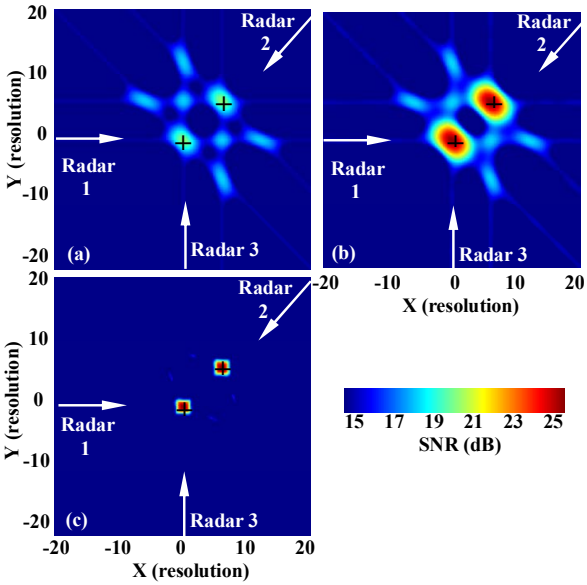


Fig. 7 Outputs of (a) noncoherent, (b) coherent, and (c) MVDR processing for the case of two targets and three radars.

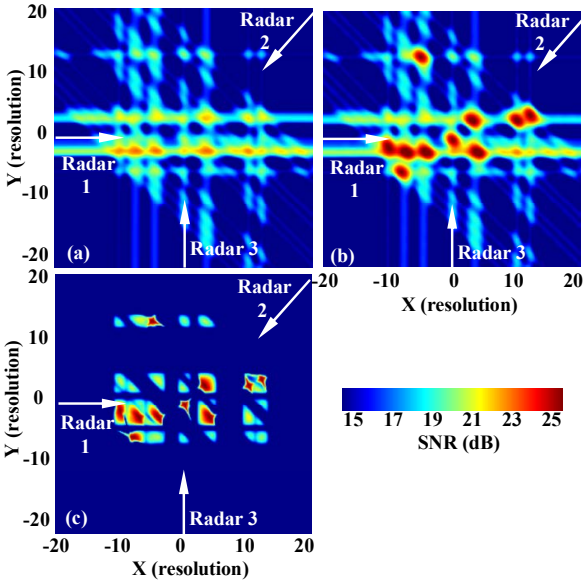


Fig. 8 Outputs of (a) noncoherent, (b) coherent, and (c) MVDR processing for the case of ten targets and three radars.

The whole radar system is synchronized in time to support coherent signal processing but each radar ultilizes an identical waveform that may be operated in a separate, disjoint frequency band. Certainly, different waveforms for different radars are feasible and sometimes preferred. Indeed, the subject matter of the waveform design and its processing are important considerations in practical implementation of the multilateral radar system operation. Conceptually, the radar in a multilateral system does not need to be monostatic, nor is it required to be active. Conceivably, the radar system may consist of a single transmitter and several receivers arranged in a SIMO (single-input, multiple-output) configuration. Or,

alternatively, the system may employ more than one set of transmitters and receivers in a MIMO (multiple-input, multiple-output) configuration [3-7]. Furthermore, in the general form, the transmitter and receiver pairs may be operated either as a monostatic or a bistatic radar. If a suite of more than one transmitter is employed, an equal number of orthogonal waveforms need to be implemented such that a receiver can receive and decode an assigned waveform without ambiguity. The collective operation of multiple radars is an active research area of high current interest. It is expected that the multilateral radar system will significantly enhance not only weak target detection but also accurate target geolocation.

## VI. CONCLUSION

In this paper, the multilateral system of several radars has been modeled to investigate the target geolocation performance. Each radar is assumed to be capable of good target range measurement but without the support of a narrow antenna beamwidth to provide any useful cross range measurement. Numerical simulations are executed to demonstrate the capability of coherent radar processing to accurately geolocate targets within about one range resolution length. The results have shown that coherent processing enhances the target signal-to-noise signature that may be profitably exploited to discriminate the real targets from their spurious ghosts. The latter capability will be difficult to implement with noncoherent processing approaches such as the conventional geometric triangulation based on target range or angle measurement. The ability of coherent multilateral processing to achieve both accurate target geolocation and ghost elimination is expected to provide significant benefits to the radar tracker that may need to be operated in a very dense target environment.

While this paper focuses on the utility of coherent multilateral processing to enhance the target signature and its geolocation, it is expected that the additional diversity of a multilateral system will offer many advantages to improve radar target detection, imaging, discrimination, and tracking as well. To restrict the scope of this paper, the current study has adopted a few simplified assumptions in modeling the target signals. Better modeling of the phenomenology of multilateral radar target scattering and propagation will be very desirable as more knowledge and measurement data become available in the future. Further, current progress in MIMO radar and communication system research also will be fertile sources of information that can be drawn upon to improve the performance of a multilateral radar system.

## REFERENCES


[1] D.R. Kirk, J.S. Bergin, P.M. Techau, and J.E. Don Carlos, "Multi-Static Coherent Sparse Aperture Approach to Precision Target Detection and Engagement," IEEE International Radar Conf., pp. 579 – 584, May 9 - 12, 2005, Arlington, VA.

[2] R. Baltes and G. van Keuk, "Tracking Multiple Maneuvering Targets In A Network of Passive Radars," IEEE International Radar Conf., pp. 304 – 309, May 8 - 11, 1995, Alexandria, VA.

[3] D.J. Rabideau and P. Parker, "Ubiquitous MIMO Multifunction Digital Array Radar," Proc. 37th Asilomar Conf. on Signals, Systems, and Computers, pp. 300 – 304, Nov. 2003, Pacific Grove, CA.

[4] R.C. Robey, S. Coutts, D. Weikle, J.C. McHarg, and K. Cuomo, "MIMO Radar Theory and Experimental Results," Proc. 38th Asilomar Conf. on Signals, Systems, and Computers, pp. 300 – 304, 2004, Pacific Grove, CA.

[5] E. Fishler, A. Haimovich, R. Blum, L. Climini, D. Chizhik, and R. Valenzuela, "Performance of MIMO Radar Systems: Advantage of Angular Diversity," Proc. 38th Asilomer Conf. on Signals, Systems, and Computers, pp. 305 – 309, 2004, Pacific Grove, CA.

[6] D.W. Bliss and K.W. Forsythe, "Multiple-Input Multiple-Output (MIMO) Radar: Performance Issues," Proc. 38th Asilomer Conf. on Signals, Systems, and Computers, pp. 310 – 315, 2004, Pacific Grove, CA.

[7] D.W. Bliss and K.W. Forsythe, "Multiple-Input Multiple-Output (MIMO) Radar and Imaging: Degree of Freedom and Resolution," Proc. 37th Asilomer Conf. on Signals Systems, and Computers, pp. 54 – 59, Nov. 2003, Pacific Grove, CA.